SME Annual Meeting
Feb. 25 - 28, 2018, Minneapolis, MN

Preprint 18-066

INVESTIGATION ON THE OVERPRESSURE PRODUCED BY HIGH-SPEED METHANE GAS DEFLAGRATIONS IN CONFINED SPACES

C. Strebinger, Colorado School of Mines, Golden, CO
M. Fig, Colorado School of Mines, Golden, CO
D. Pardonner, Univ. of West Florida, Pensacola, FL
B. Treffner, Red Rocks Community College, Lakewood, CO
G. Bogin, Colorado School of Mines, Golden, CO
J. Brune, Colorado School of Mines, Golden, CO

ABSTRACT

Methane gas explosions in a longwall coal mine can originate from in or around the gob and can seriously harm nearby workers and equipment. In order to fully understand the explosion flame and pressure wave propagation in the mine, it is important to investigate methane flame propagation in confined spaces as well as flame interaction with rock rubble and other mine structures. The latter can lead to enhanced turbulence causing high-speed deflagrations and/or detonations. Researchers ignited methane-air mixtures in horizontal, cylindrical reactors that contained inserts to simulate various gob characteristics. Rock surface topology and ignition location were investigated. Results show rock surface roughness increased fluid motion, thereby increasing methane flame front propagation velocity, overall pressure rise of the explosion, and time of pressure decay. Moving the point of ignition away from the open end of the reactor resulted in an increase in peak overpressure and an overall pressure rise of the explosion. Experiments were used to validate a computational fluid dynamics (CFD) combustion model that will be incorporated into a mine-scale explosion model to simulate and predict explosion hazards of large scale methane gas deflagrations in longwall coal mines.

INTRODUCTION

Coal mining is an integral part to our global society with coal-fired power plants providing about 40% of our global electricity [1]. A common method of extracting coal underground is by longwall mining. Researchers and investigative reports have found that explosive gas zones of methane-air mixtures can form along the longwall face and within the longwall gob, presenting an explosion risk to nearby workers and equipment [2]. In an explosion, the resulting flame and pressure wave presents a fatal traumatic injury hazard and can cause serious damage to equipment. In order to evaluate and mitigate the explosion risks in longwall coal mining, researchers at the Colorado School of Mines are developing a coupled CFD and combustion model of a longwall coal mine. The purpose of the model will be to better predict the explosion hazards under various mine conditions in order to build stronger prevention and mitigation strategies for miners.

A main focus of the combustion model is to develop a fundamental understanding of the coupling of pressure waves and flames produced by methane gas deflagrations in confined spaces. This is important since a methane gas explosion in the gob or near the longwall face is analogous to ignition in a confined space. Confinement is known to greatly enhance methane flame propagation due to the increased temperatures, pressures, and enhanced fluid motion [3]. Understanding the resulting pressure rise and flame interaction from a methane explosion is also important for determining the risk for traumatic and burn injuries as well as impact on mine structures. It is the goal of this research to fundamentally understand the pressure effects of high-speed methane gas deflagrations in confined spaces and through rock rubble. This paper will discuss the background on pressure generation and flame dynamics, provide detail on the experimental and model setups, discuss results of confined methane gas explosions, and the importance of these findings for longwall coal mining.

BACKGROUND

Pressure generation from gaseous explosions has been investigated for decades and has important applications in many different industrial settings including longwall coal mining [4-16]. Fundamentally, explosions require fuel, oxygen, heat, ignition, dispersion, and confinement. If any of these five elements of the explosion pentagon is missing, the explosion will not occur. In industrial processes, venting is often used to help eliminate confinement thereby preventing or reducing pressure build-up. Researchers have found there are many factors that affect pressure generation including vessel size/geometry [4,7,11,14,15], ignition location [4,6,10,11,15], and fuel type and concentration [4,6,8,10,11,16]. Studies show pressure development and flame dynamics are coupled through hydrodynamic instabilities [4,5,6,7,11,15], acoustic interactions [4,7,11,15,16], and obstacle induced turbulence leading to enhanced combustion [10,13,14]. However, Bradley and Mitcheson [5,6], Bauwens et al. [11], and Fairweather et al. [13] found that accurately modeling the coupling between pressure and flame dynamics is difficult. Furthermore, previous experimental research discussed here uses varying set-ups and to date, these researches have not found methane flame or pressure data with ignition between obstacles (i.e. ignition from within the gob). It is the goal of this research to better understand the coupled pressure and flame dynamics of explosions in confined spaces in order to build a fundamental CFD combustion model and in the future, simulate a physically accurate longwall coal mine explosion. To study this, experiments were performed in a cylindrical reactor varying parameters such as fuel concentration, ignition location, vent size, and obstacle material as will be described in this manuscript.

EXPERIMENTAL SETUP & PROCEDURE

Due to safety concerns of performing methane gas explosions in a full-scale experimental mine, researchers at the Colorado School of Mines perform experiments in a series of horizontal cylindrical flow reactors with diameters ranging from 5 cm to 71 cm and lengths of 1.2 m to 6.1 m [3,17,18]. By measuring the flame front propagation velocity, flame shape, pressure rise, and other parameters, researchers validate CFD combustion models which can then be extended to simulate large-scale methane gas explosions in a longwall coal mine. The large explosion reactor with diameter 71 cm and length 6.1 m provides a more accurate representation of methane explosions in a real mine. Smaller-scale, laboratory experiments can be performed with less methane and air in shorter times to help determine fundamental flame propagation properties before moving to the larger reactor.

This manuscript presents a series of experiments performed in a 12.5 cm outer diameter, 1.5 m long horizontal cylindrical quartz reactor schematically shown in Figure 1. The quartz flow reactor allows full visualization of the flame as it transitions from ignition to a flame kernel

and into a laminar and turbulent flame. The quartz flow reactor has one end open to atmosphere while the other end is closed using an aluminum plate with several relief holes (Figure 1). Each relief hole is 1 cm in diameter and may be open or plugged, as specified. A Kistler© 4260A piezoresistive pressure transducer is mounted on the aluminum plate to record the pressure rise in the reactor during the explosion. Figure 1 also shows 5 ports spaced 25 cm apart along the top of the reactor. These ports house ion sensors that detect the flame front to measure its propagation velocity.

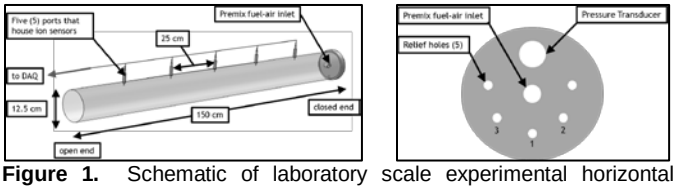

Figure 1. Schematic of laboratory scale experimental horizontal quartz flame reactor (left) and closed end of the reactor (right). Diameter of each relief hole on the closed end is 1 cm.

The experimental set-up consists of compressed methane and zero-grade air cylinders, mass flow controllers, a mixing chamber, and the horizontal flow reactor described in previous publications [3,17,18]. During filling of the methane-air mixture, the open end of the reactor is covered with aluminum foil in order to contain the combustible gas. A small perforation in the foil allowing ambient air to escape the cylinder during filling. Note there is minimal pressure required to remove the aluminum foil during a combustion event.

Methane flow is controlled by an Alicat Scientific MC Series (0-5 SLPM) mass flow controller and air flow is controlled by a Bronkhorst EL-FLOW Select (0-50 SLPM) controller. Methane and air are combined in a mixing chamber to ensure a homogenous gas mixture. Homogeneity is confirmed by an Infrared Industries IR-6000 gas analyzer and methane content of the mixture is verified by a gas chromatography using thermal conductivity detection. From the mixing chamber, the gas flows into the quartz reactor for 5 minutes at approximately 200 kPa, flowing at least 2 times the volume of the reactor. The mixture then settles for 40 seconds, ensuring stagnant conditions prior to ignition. After opening the desired number of relief holes, combustion is initiated using an automotive spark ignition system that provides a spark of approximately 60 mJ. After the experiment, combustion products are flushed out using compressed air until the reactor is cooled to ambient conditions. Each experiment is performed at a temperature and pressure of 293 K and 83 kPa for Golden, Colorado - elevation 1,730 m above sea level.

Data is recorded using electronic data acquisition systems. The ion sensors are wired to a NI USB-6008 DAQ board and the pressure transducer is wired to a NI USB-6009 DAQ board both capable of sampling at 48,000 samples per second. To ensure repeatability, each experimental setup is run 4-5 times with the same parameters. Flame front propagation velocities reported are the average of all experimental runs and the error bars represents the standard deviation of the mean.

EXPERIMENTAL PARAMETERS

To build a comprehensive understanding of methane combustion in confined spaces, the following parameters were investigated: mixture stoichiometry, ignition location, venting area, and obstacle material:

- Mixture stoichiometry was 7.5±0.3%, 9.5±0.3% or 11.5±0.3% methane in air, by volume.
- Ignition location was varied along the length of the reactor, centered radially, as follows:
  - Open-end ignition: ignition 11 cm from open end of reactor.
  - Closed-end ignition: ignition 11 cm from closed end of reactor.
  - Port 1 ignition: ignition 25 cm from open end of reactor.
  - Port 2 ignition: ignition 50 cm from open end of reactor.
  - Port 3 ignition: ignition 75 cm from open end of reactor.
  - In-gob ignition Port 1: ignition 25 cm from open end of the reactor, centered between two obstacles as shown in Fig. 2.
- Venting area was varied by changing the number of relief holes on the closed end of the quartz reactor (1 hole = 0.78 cm^2) as shown in Figure 1. Note: 1 hole corresponds to '1', 2 holes is hole '1' and '2'.
- Figure 3 shows the obstacles used in this study, which have been previously described by Strebinger et al. [3]:
  - Mesh: A non-reacting steel cage with 6.35 mm spacing. The cage is flush with the inside of the reactor having a diameter of 12 cm and length of 2.54 cm.
  - Glass and granite obstacle: 6.35 mm diameter smooth glass spheres and 7.75 ± 0.53 mm granite pebbles were oriented in a checkerboard pattern using a metal mesh as shown in Figures 2 and 3. The obstacle has a porosity of 77% and constant void spacing.

It is noted that granite pebbles and glass have similar thermal conductivities (approximately 1 to 1.5 W/m^2-K). The major difference between the glass and granite pebbles used in this study is the surface roughness of the granite - this will be discussed later.

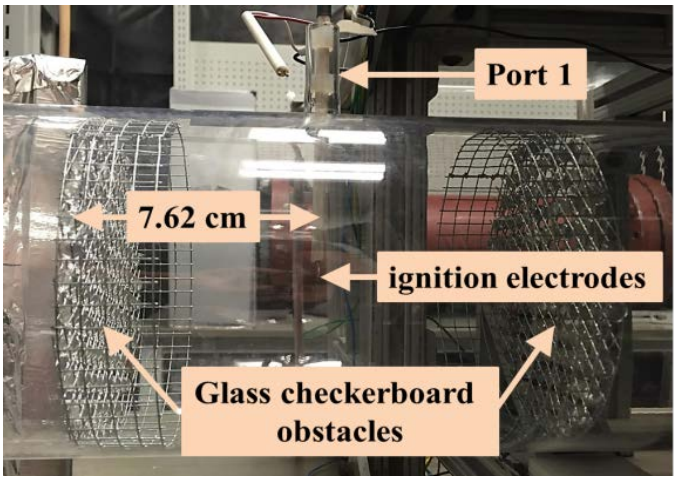

Figure 2. Image of in-gob ignition in Port 1 with glass checkerboard obstacles separated 7.62 cm on either side of the ignition electrodes.

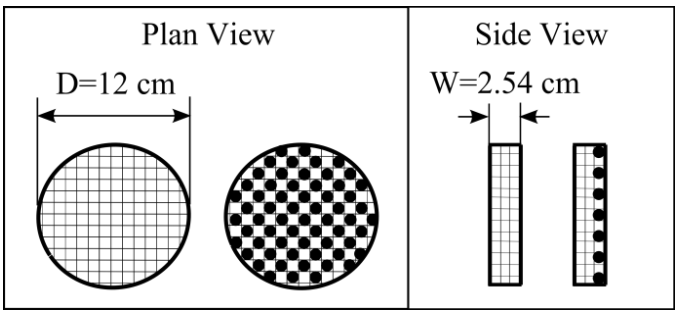

Figure 3. Schematic of obstacle geometries used in this study. Left: Wire mesh, Right: Glass or granite checkerboard.

NUMERICAL MODEL SETUP

Researchers at the Colorado School of Mines developed CFD and combustion models using ANSYS Fluent [17,18]. The combustion model assumes a 2-D planar geometry and has been validated under many experimental conditions as described by Fig et al. [17, 18]. The geometry of the model has been modified for the quartz flow reactor presented in this work; the height of the model is 12.5 cm and length is 1.5 m. Researchers also performed a mesh independence study, concluding that a body mesh size of 1 mm is sufficient. The current model initially uses a simplified 2-step combustion mechanism in order to obtain a general understanding of methane flame propagation

trends. Modeling using the full GRI 1.2 mechanism [20] will be performed at a later stage of the project.

The following settings were used in ANSYS Fluent:

- 2-D, compressible flow
- Viscous-Standard **k-ω** model
- Time Step = 0.1 milliseconds
- Body Mesh Size = 1 mm
- Second order implicit time solver
- Methane-air 2 step mechanism
- SIMPLE pressure-velocity coupling
- Ideal gas for density changes
- Kinetic theory for gas mass diffusivity
- Adaptive meshing on gradient of kinetic rate
- Convergence criteria were set to 10^{-6}, except mass which was set to 10^{-4}
- Spark was modeled as an aluminum point source representing the spark electrodes.
- Model operating conditions, T and P, were run at typical lab conditions.

The checkerboard geometries were modeled as spheres or granite pebbles centered on a vertical line 7.62 cm on either side of the spark location. The spheres were modeled with a diameter of 6.35 mm and a no slip boundary condition on the surface. The granite pebbles were modeled as irregular shapes as shown in Figure 4 with no additional surface roughness and a no slip boundary condition. The diameter of the circle enclosed inside the rock is 4.6 mm and the average height, L, of the irregularities is 1.7 ± 0.3 mm. At this stage, no quantitative method was used to more precisely describe the shape of the irregular rocks. In the future, researchers will be using quantitative methods.

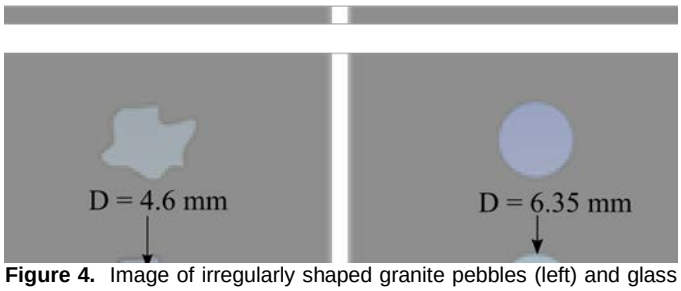

Figure 4. Image of irregularly shaped granite pebbles (left) and glass spheres (right) used for comparison of in-gob ignition models. Thermal properties of granite were used. Note: not to scale

RESULTS AND DISCUSSION

Table 1 shows the flame front propagation velocities measured in an open-end and closed-end ignition across a range of methane-air mixture concentrations. Results show the maximum flame front propagation velocities correspond to a methane-air mixture of 9.5% methane by volume which agrees with fundamental theory [19]. Closed-end ignition results in flame front propagation velocities approximately 45 times higher than those in an open-end ignition. The increase is due to inadequate venting resulting in higher temperatures, increased fluid motion ahead of the flame, and increased pressures generated by the explosion.

Figure 5 compares the pressure-time history of an open-end ignition (red) versus a closed-end ignition (blue). The pressure history of a closed-end ignition (blue) shows two distinct peak pressures followed by oscillations. These peaks are in agreement with the first two fundamental peaks found by Cooper et al. [4] shown in Figure 6. The first peak pressure rise, P_1, is the result of the initial kernel expansion when the production of combustion gases exceeds the volume removed by venting [4]. The second major pressure peak, P_2, occurs after initial venting [4] when the flame front ignites unburned gases increasing the rate of combustion and pressure rise in the vessel [4]. After the second peak, Helmholtz modes are excited and the flame front undergoes bulk motion [4, 7]. Bradley and Mitcheson [5] discuss venting of burned and unburned gases and concluded that when burned gases are vented "the maximum pressure might tend to be lower" which agrees with these findings (Figure 5).

Table 1. Table of maximum flame front propagation velocities of open-end versus closed-end ignition for various methane-air mixture concentrations.

	Maximum Flame Front Propagation Velocity (cm/s)	
Methane %	Open-end Ignition	Closed-end Ignition
7.5	105 ± 1.5	4029 ± 66.1
9.5	128 ± 0.95	6464 ± 122
11.5	95.0 ± 6.3	4306 ± 129

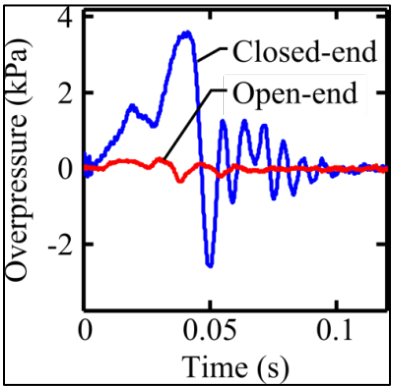

Figure 5. Pressure-time history of a closed-end ignition (P_{max} = 3.25 ± 0.07 kPa) versus open-end ignition (P_{max} = 0.26 kPa). CH_4 = 9.5%. Operating conditions 293 K, 83 kPa. One (1) relief hole.

Figure 6 also shows two additional pressure peaks, P_3 and P_4. After the Helmholtz oscillations, the flame expands, turbulence and combustion increases, and large density gradients are created in the vessel which increases the pressure, P_3 [4]. Finally, as the production of burned gases decreases, the pressure in the vessel decreases and couples "with the acoustic modes of the vessel" sustaining pressure oscillations creating a high frequency fourth peak, P_4 [4, 16]. These researchers have not observed the third pressure peak and have only observed the fourth pressure peak in some of the experiments presented in this paper. However further studies must be performed before discussing these peaks.

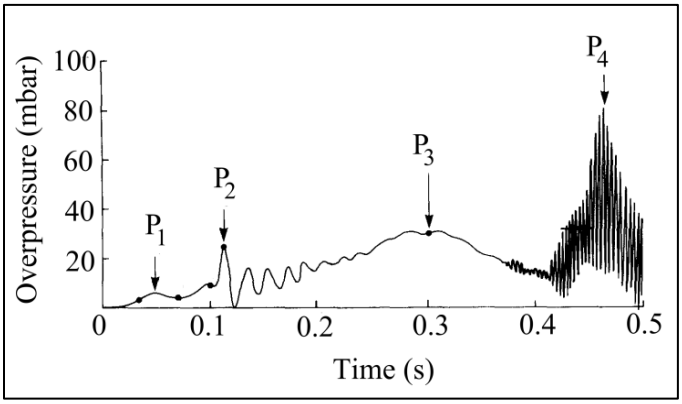

Figure 6. Example of a typical pressure-time profile of an explosion in a near cubic vessel with a single vent. SOURCE: Modified from Reference [4].

Figure 7 shows the pressure-time history of a closed-end ignition for various mixture concentrations. As expected the 9.5% (green)

stoichiometric mixture produced the largest pressure rise, P_2, which agrees with other researchers [8,10]. In this case, peak P_2 is approximately twice that of the lean (red) or rich (blue) cases, respectively.

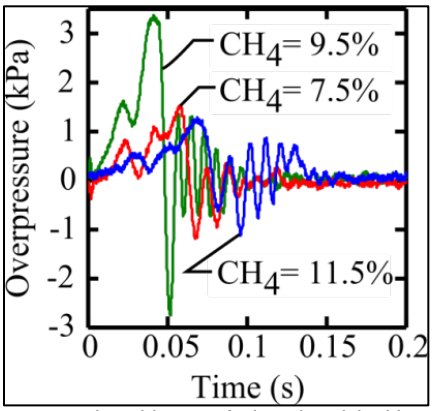

Figure 7. Pressure-time history of closed-end ignition with varying mixture stoichiometry. Ignition 11 cm from closed end. $P_{max}(CH_4 = 9.5\%) = 3.25 \pm 0.07$ kPa. $P_{max}(CH_4 = 7.5\%) = 1.54 \pm 0.04$ kPa. $P_{max}(CH_4 = 11.5\%) = 1.38 \pm 0.26$ kPa. Operating conditions 293 K, 83 kPa. One (1) relief hole.

In the next set of experiments the ignition location was varied along the length of the reactor in Ports 1, 2, and 3 (ignition 25, 50, and 75 cm from the open end respectively) – see Figure 1. Figure 8 demonstrates the influence of ignition location. As ignition is moved further from the open end, the maximum flame front propagation velocity increases. Figure 9 shows that the pressure in the explosion vessel increases as the ignition point moves away from the open end towards the center of the vessel which agrees with previous researchers [4,6]. Ignition within Port 3 was centered in the quartz reactor and produced the largest pressure rise. This confirms observations in published literature where central ignition was found to produce the largest pressure rise [6,10].

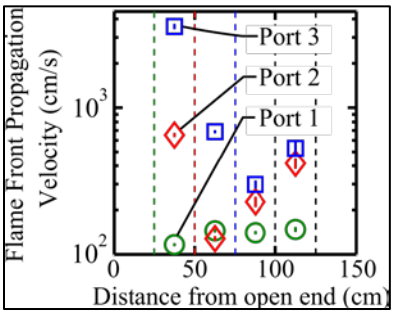

Figure 8. Impact of ignition location on methane flame front propagation velocity. *Green:* ignition in sensor port 1 (25 cm from open end), *Red:* ignition in sensor port 2 (50 cm from open end), *Blue:* ignition in sensor port 3 (75 cm from open end). Dotted lines represent flame detector locations – *colors correspond to ignition within the respective port*. CH_4 = 9.5%. Operating conditions 293 K, 83 kPa. One (1) relief hole. Standard deviations range: 0.43 – 85 cm/s.

Researchers found that ignition in Port 2, 50 cm from the open end of the reactor, can cause a higher pressure rise in the reactor than a closed-end ignition, but has a slower flame front propagation velocity. The duration of the pressure-time history of ignition in Port 2 is longer than that for a closed-end ignition. These differences are mainly due to the large acoustical waves produced by explosion, which in the case of ignition in Port 2, continue to interact with the walls of the vessel and flame front thereby increasing the overall pressure rise. This result is important because in a real longwall coal mine, pressure waves may travel throughout the mine, reverberate off walls and interact with other mine structures and thus increase the overpressure. Pressure waves can inflict traumatic injuries and throw workers, interfere with ventilation controls, and stress mine structures [2,12].

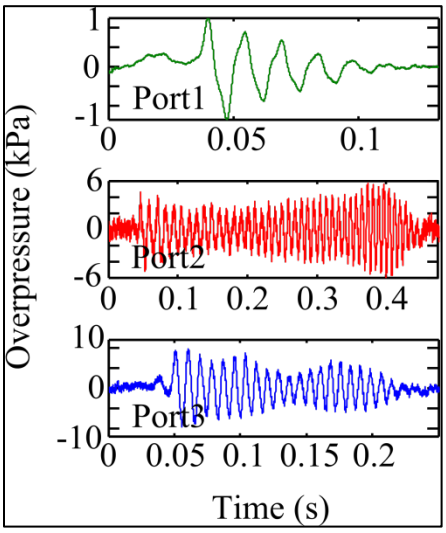

Figure 9. Pressure-time history of ignition within various ports. *Top:* Ignition in sensor port 1 (25 cm from open end), $P_{max}= 1.23 \pm 0.05$ kPa. *Middle:* Ignition in sensor port 2 (50 cm from open end), $P_{max}= 5.69$ kPa. *Bottom:* Ignition in sensor port 3 (75 cm from open end), $P_{max}= 8.59 \pm 1.8$ kPa. CH_4 = 9.5%. Operating conditions 293 K, 83 kPa. One (1) relief hole.

In order to directly compare the experimental results shown in Figure 8 to CFD results, the maximum flame front propagation velocity between sensors 4 and 5 was normalized to Port 1. These were compared to the normalized maximum flame front propagation velocity towards to the closed end from CFD results shown in Table 2. The normalized data further demonstrates that as ignition is moved further from the open end, the flame front velocity increases. The differences between the experimental and numerical data can be attributed to the fact that a simplified combustion model was used. Additionally, acoustic effects have not yet been considered in the model.

Table 2. Comparison of normalized flame front propagation velocity between ports 4 & 5 shown in Figure 9 to CFD results. CH_4 = 9.5%. Mesh cell size = 0.001m.

	Normalized Flame Front Propagation Velocity	
Port	Numerical	Experimental
1	1.0	1.0
2	2.1	2.8
3	2.8	3.6

Researchers also varied the location and number of vents in the closed end of the reactor. Guo et al. [9] experimented with two vents opposite each other, but comparison is difficult as they used different gases and a different experimental setup. The cases shown in Figures 10 and 11 are for ignition in Port 2 with varying the number of relief holes in the closed end of the reactor. Similar to previous findings, increasing the venting area can help reduce the overpressure [4-7,9,11,15] and the flame front propagation velocity towards the closed end of the reactor [11]. However, it was found for this experimental setup that as venting area decreases, pressure oscillations are sustained at a greater magnitude and for longer durations which is important because pressure waves greater than 35kPa can severely harm human ear drums [2]. Sustained high pressures can also reverse airflow in a mine, destroy ventilation controls, and displace mine structures [2,12]. This research demonstrates that even small changes to confinement relief openings directly impact methane flame dynamics and pressure. This is an important fundamental mechanism to capture in a CFD model.

Researchers found no measureable change in flame front propagation velocity or peak pressure in a closed-end ignition, CH_4 =

9.5%, when the number of relief holes was changed from 0-4 because the expansion of the reaction gases is greater than the volume of unburned gases vented from the closed end.

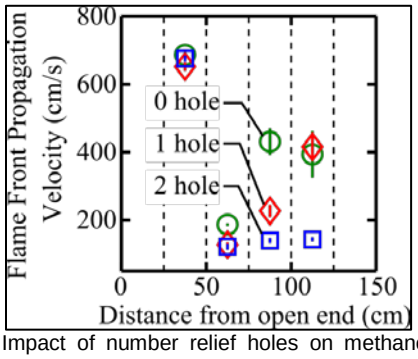

Figure 10. Impact of number relief holes on methane flame front propagation velocity for ignition in sensor port 2 (50 cm from open end). Dotted lines represent flame detector locations. CH_4 = 9.5%. Operating conditions 293 K, 83 kPa. Standard deviation range: 0.23 – 65 cm/s.

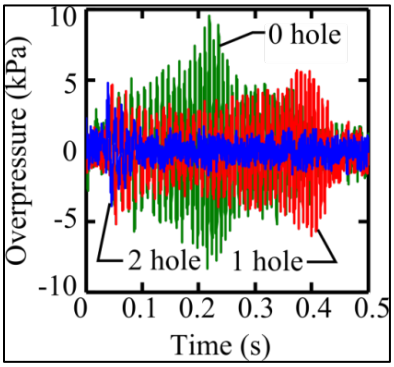

Figure 11. Impact of number relief holes on pressure rise for ignition in sensor port 2 (50 cm from open end). Dotted lines represent flame detector locations. P_{max}(0 hole) = 11.2 ± 1.0 kPa, P_{max}(1 hole) = 5.69 kPa, P_{max}(2 hole) = 4.49 ± 0.51 kPa. CH_4 = 9.5%. Operating conditions 293 K, 83 kPa.

A simplified experiment of an in-gob ignition was carried out with the ignition electrodes placed between two "rock walls" with a porosity of 77%, as shown in Figure 2. Initial results have shown that there is a competing effect of induced turbulence by an obstacle and the pressure restriction from the obstacle [3]. Results in Figure 12 show that ignition between two wire mesh obstacles enhances turbulence in nearby unburned gases which helps accelerate the flame within 25 cm upstream of the obstacles. The glass spheres induce movement in nearby gases, but the pressure restriction from the obstacle slows the flame down as compared to the empty wire mesh. Furthermore, granite pebbles, due to their surface roughness, induce more fluid movement in the nearby gases resulting in higher flame front propagation velocities in the first 25 cm as compared to the glass spheres. Further downstream of the obstacles, the induced turbulence diminishes and the flame front propagation velocities approach a similar value due to the pressure resistance experienced by the flame from the closed end of the reactor.

Obstacles have a large impact on the pressure-time history inside the quartz reactor as shown in Figure 13. The granite pebbles produced the highest peak pressures for the longest duration, followed by the glass spheres, and the empty wire mesh. Though the experimental set-ups vary, these results agree with previous researchers who found obstacles can increase overpressure [10,14], enhance turbulence [13,14], and promote combustion and burning velocity [10,13,14]. The decay of the pressure waves after the second major peak is greatest for the glass spheres, followed by the wire mesh and the granite pebbles. These results help to confirm that the granite pebbles increases mixing for a longer period of time in the unburned gases allowing for more complete combustion and faster flame front propagation.

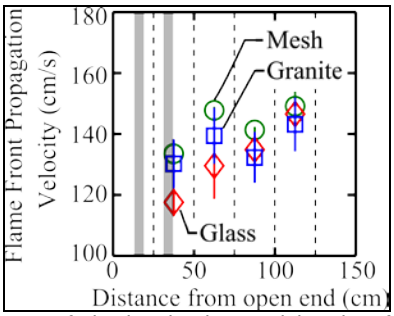

Figure 12. Impact of simulated gob material and surface roughness on methane flame front propagation velocity for in-gob ignition in sensor port 1 (25 cm from open end). Obstacle location 7.62 cm on either side of ignition represented by gray bars. Obstacle: wire mesh, 6.35 mm diameter glass spheres, averaged 7.75 ± 0.53 mm diameter granite pebbles. Dotted lines represent flame detector locations. CH_4 = 9.5%. Operating conditions 293K, 83kPa. One (1) relief hole. Standard deviation range: 0.69 – 8.8 cm/s.

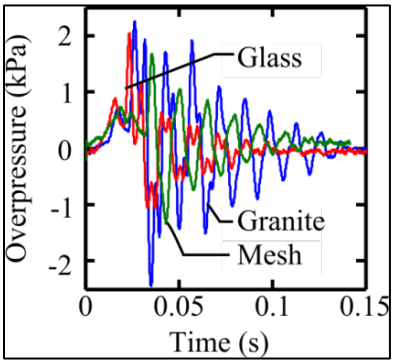

Figure 13. Pressure-time history of in-gob ignition in sensor port 1 with varying obstacle surface roughness (ignition 25 cm from open end). Obstacle location 7.62cm on either side of ignition. Obstacle: wire mesh (P_{max} = 1.59 ± 0.05 kPa), 6.35 mm diameter glass spheres (P_{max} = 2.05 ± 0.01 kPa), averaged 7.75 ± 0.53 mm diameter granite pebbles (P_{max} = 2.18 ± 0.02 kPa). CH_4 = 9.5%. Operating conditions 293 K, 83 kPa. One (1) relief hole.

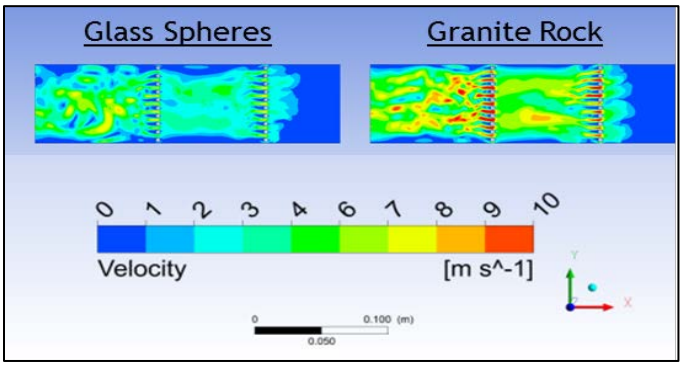

Figure 14. Velocity contours of CFD model at t = 0.08s of in-gob ignition between glass spheres (left) and granite pebbles (right) in a checkerboard geometry. CH_4 = 9.5%. Mesh cell size = 0.001m.

The in-gob ignition experiments were reproduced in the combustion CFD model as shown in Figures 14 and 15 and agree with the results and conclusions in the experiments shown in Figures 12 and 13. The CFD results show greater fluid velocities across the granite pebbles and more complete conversion of methane and air to CO_2 as compared to the glass sphere model which shows pockets of CO demonstrating incomplete combustion. These results indicate that even small changes in surface topology (roughness of the granite) can

greatly promote fluid motion and combustion, leading to faster flame front propagation velocities and pressure rises. These results are important because previous research has found that the dynamic pressure can also have a large effect on mine structures [12]. Additionally, these results are important further validating the combustion model since the gob material in longwall coal mine is made up of broken rocks in irregular shapes and sizes.

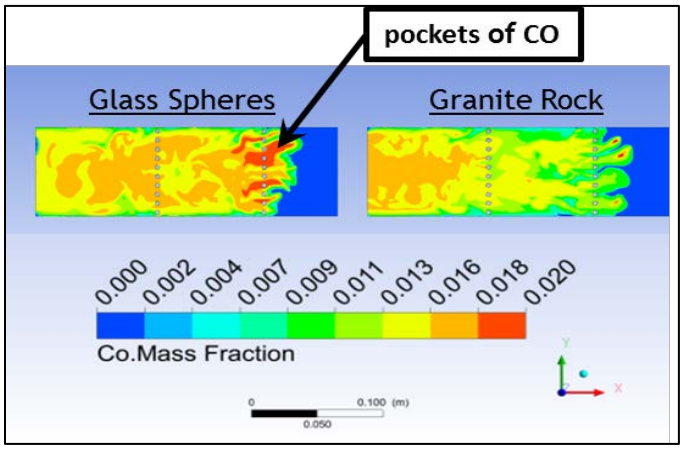

Figure 15. CO mass fraction contours of CFD model at t = 0.08s of in-gob ignition between glass spheres (left) and granite pebbles (right) in a checkerboard geometry. CH_4 = 9.5%. Mesh cell size = 0.001m.

CONCLUSIONS

Experiments performed in a small scale horizontal quartz flow reactor show that methane flame propagation and pressure wave propagation significantly depend on ignition location, venting size, and physical characteristics of the obstacles simulating rock rubble. Results from this study show that ignition from a confined space can greatly enhance methane flame front propagation velocity and overall pressure rise of the explosion. Previous researchers have found that for a vessel with one vent, central ignition produces the largest pressure rise [6,10]. This study agrees with previous research, but also found that ignition locations between the main vent and center of the vessel can produce overpressures greater and with a longer duration than a closed-end ignition. Increased area of the vents at the closed end can decrease the peak pressure rise depending on ignition location. Results show that ignition within obstacles, i.e. within a longwall gob, can increase peak overpressure. The amount of pressure restriction of the obstacle can help reduce the overpressure, but increased roughness of the obstacle surface can increase pressure and burning velocities due to the enhanced fluid motion. These results have been replicated in a CFD combustion model which aids in understanding the impact of a nearby obstacle on methane gas combustion dynamics, showing that a rough obstacle surface can enhance mixing of gases and promote an accelerated combustion event.

These results have important implications for longwall coal mining since methane gas explosions can occur in gob areas with varying levels of rock compaction and porosity. Results from this research demonstrate that there is a need to perform further research to fundamentally understand the contributing factors to pressure wave generation from methane explosions in mines by exploring the effects of multiple open pathways and obstacles on methane gas deflagrations. Researchers will use the results of this work to validate a coupled CFD and combustion model for modeling large-scale longwall coal mine gas explosions. Developing a combustion model capable of capturing complex processes such as the coupling of flame and pressure dynamics from explosions is vital to further understanding the effects of large-scale methane gas explosions in longwall coal mines.

ACKNOWLEDGEMENT

This research is made possible with the support from the National Institute for Occupational Safety and Health (NIOSH) Contract # 211-2014-60050.

REFERENCES

1. World Coal Association. 2017, February 21. “Basic coal facts.” Retrieved October 2017, https://www.worldcoal.org/basic-coal-facts
2. Brune, J., “The methane-air explosion hazard within coal mine gobs”, SME Transcript 334, October 2013.
3. Strebinger, C, Fig, M, Bogin, Jr., G. E., Brune, J. F., Grubb, J. W. “Effect of Simulated Gob Conditions on the Burning Velocity of Premixed Methane-Air Combustion”, SME Annual Conference and Exhibit. Denver, CO. February 2017.
4. Cooper, M. G., Fairweather, M., Tite, J. P. “On the Mechanisms of Pressure Generation in Vented Explosions”, Combustion and Flame 65, pp 1- 14, 1986.
5. Bradley, D. and Mitcheson, A., “The Venting of Gaseous Explosions in spherical Vessels. I – Theory”, Combustion and Flame 32, pp 221-236, 1978.
6. Bradley, D. and Mitcheson, A., “The Venting of Gaseous Explosions in spherical Vessels. II – Theory and Experiment”, Combustion and Flame 32, pp 237-255, 1978.
7. McCann, D. P. J., Thomas, G. O., Edwards, D. H., “Gasdynamics of Vented Explosions Part I: Experimental Studies”, Combustion and Flame 59, pp 233-250, 1985.
8. Bao, Q., Fang, Q., Zhang, Y., Chen, L., Yang, S., Li, Z, “Effects of gas concentration and venting pressure on overpressure transients during vented explosion of methane-air mixtures”, Fuel 175, pp 40-48, 2016.
9. Guo, J., Wang, C., Liu, X., Chen, Y., “Explosion venting of rich hydrogen-air mixtures in a small cylindrical vessel with two symmetrical vents”, International Journal of Hydrogen Energy 42, pp 7644-7650, 2017.
10. Kindracki, J., Kobiera, A., Rarata, G., Wolanski, P., “Influence of ignition position and obstacles on explosion development in methane-air mixtures in closed vessels”, Journal of Loss Prevention in the Process Industries 20, pp 551-561, 2007.
11. Bauwens, C. R., Chaffee, J., Dorofeev, S., “Experimental and Numerical Study of Methane-air Deflagrations in a Vented Enclosure”, Fire Safety Science – Proceedings of the Ninth International Symposium, pp1043-1054, 2008.
12. Zhang, Q., Ma, Q. J., “Dynamic pressure induced by a methane-air explosion in a coal mine”, Process Safety and Environmental Protection 93, pp 233-239, 2015.
13. Fairweather, M., Hargrave, G. K., Ibrahim, S.S., Walker, D.G., “Studies of Premixed Flame Propagation in Explosion Tubes”, Combustion and Flame 116, pp 504-518, 1999.
14. Moen, J., Lee, B. Hjertager, K. Fuhre, R. Eckhoff, “Pressure development due to turbulent flame propagation in large-scale methane-air explosions”, Combustion and Flame 47, pp 31-52, 1982.
15. Solberg, D. M., Pappas, J. A., Skramstad, E., “Observations of flame instabilities in large scale vented gas explosions”, Proceedings of the Eighteenth International Combustion Symposium, The Combustion Institute, pp 1607-1614, 1981.
16. vanWingerden, C. J. M., Zeeuwen, J. P., “On the Role of Acoustically Driven Flame Instabilities in Vented Gas Explosions and Their Elimination”, Combustion and Flame 51, pp 109-111, 1983.
17. M. Fig, G. Bogin, J. Brune, J. Grubb, “Experimental and numerical investigation of methane ignition and flame propagation in cylindrical tubes ranging from 5 to 71 cm – Part I: Effects of scaling from laboratory to large-scale field studies”, Journal of Loss Prevention in the Process Industries 41, pp 241-251, 2016.

18. Fig, M, Bogin, Jr., G. E., Brune, J. F., Grubb, J. W., "The Effect of Environmental Factors on the Propagation of Methane Flames in the Longwall Gob". 16th North American Mine Ventilation Symposium, June 2017.

19. Turns, S. R., "An Introduction to Combustion: Concepts and Applications", McGraw Hill, 3rd Edition, 2012.

20. A. Kazakov and M. Frenklach, http://www.me.berkeley.edu/drm/ (Accessed 11/01/2017)